Korean J. Chem. Eng., 38(2), 276-291 (2021)
DOI: 10.1007/s11814-020-0683-2

pISSN: 0256-1115
eISSN: 1975-7220

Carbon adsorbents for methane storage: genesis, synthesis, porosity, adsorption

Ilya Men'shchikov†, Andrey Shiryaev, Andrey Shkolin, Vladimir Vysotskii, Elena Khozina, and Anatoly Fomkin

A.N. Frumkin Institute of Physical Chemistry and Electrochemistry of the Russian Academy of Sciences (IPCE RAS), Leninskii Prospect, 31, Building 4, Moscow, 119071, Russia

(*Received 8 June 2020 • Revised 19 September 2020 • Accepted 21 September 2020*)

Abstract−Adsorbed natural gas (ANG) storage systems are based on nanoporous adsorbents with a tailored porous structure. Activated carbons are among the most promising and widely used candidates for this application, which is explained by the availability and abundance of raw material resources. In the present work, several series of activated carbons prepared from various precursors (coconut shell, peat, polymers, silicon carbide, and mineral coal) by different routes of physical and thermochemical activation were considered in the context of the adsorbed natural gas storage applications. Based on the Dubinin theory of volume filling of micropores and BET method, the porous structure of these adsorbents was evaluated from standard adsorption isotherms. The XRD, SAXS, and SEM measurements revealed variations in the textural and morphological properties of the adsorbents and their dependence on the precursor and synthesis procedure. The pore sizes evaluated from the adsorption and SAXS data were compared. Experimental data on methane adsorption at the temperature of 303 K and pressures of 0.1, 3.5, and 10 MPa made it possible to identify the most effective adsorbents. It was shown that the adsorption properties of ACs prepared from peat and mineral coal are determined by surface chemistry inherited from the precursor and activating agent. In contrast, the adsorption performance of ACs from polymer and coconut shell depends solely on the pore volume and pore dimensions. The adsorption effectiveness of each AC varies with pressure as a function of textural properties. Thus, a selection of an optimal adsorbent should be adjusted for thermodynamical coditions of ANG system.

Keywords: Adsorbed Natural Gas Storage, Activated Carbon, Adsorption Theory of Volume Filling of Micropores, X-ray Measurements, Scanning Electron Microscopy, Methane Adsorption

INTRODUCTION

Adsorption methods of storage and transportation of energy gases, such as methane and hydrogen, are of great applied interest [1-8]. The storage of adsorbed natural gas (methane) in pores of an adsorbent (ANG technique) has several advantages over widely used conventional techniques as compression and liquefying of natural gas [1-5].

A microporous adsorbent with proper porosity, providing a sufficiently high methane adsorption capacity, is an essential element of an ANG system [6]. Among adsorbents, activated carbons (AC) are the only commercially viable material for ANG in terms of mature technologies of their production at an industrial scale. Numerous studies demonstrated the excellent adsorption properties of AC relative to methane combined with their stability, hydrophobicity, and sufficient mechanical strength [3,5-9].

Recently, numerical simulations have shown that the formation of a proper porous structure is a mandatory step to increase the efficiency of methane accumulation in ACs [10-13]. Of note is that the packing density of spherical molecules in slit-like micropores of ACs is higher than in cylindrical micropores [6]. The highest density of methane adsorbed in slit-like pores of a model carbon adsorbent at pressures above 3.5 MPa is achieved when the pore width ranges from 1.0 to 1.2 nm [10-12]. Molecular dynamics showed that at 273 K density of adsorbed methane has maxima at slit pore sizes of 0.7, 1.0-1.1, and 1.4 nm [13]. The highest density and, accordingly, the highest adsorption is reached when the pore width ranges from 1.0 to 1.2 nm [10-12], i.e., in the case of two-molecule thick layer micropore filling. In this case, the distance between methane molecules in the layer is very close to the distance between methane molecules and the nearest pore wall, and the void spaces are minimal.

Real carbon adsorbent is a solid material with a hierarchical porous structure reaching a specific surface area over 1,000 m^2/g, characterized by a variable pore size distribution and versatile surface chemical properties [6,14]. For example, two ACs of equal weight prepared from various raw materials or by different methods may possess the same total surface area but function differently as adsorbents. Indeed, as shown in [15,16], it is impossible to compare experimental data on methane adsorption capacity from different research groups solely based on the interfacial surface. One reason is that the specific surface area evaluated by the Brunauer-Emmett-Teller (BET) method - S_{BET} [17], has no physical sense for microporous adsorbents and, thus, it can be used as a "fingerprint" for comparison [18]. Indeed, adsorption in microporous adsorbents does not always proceed by the successive formation of adsorption layers on the micropore surface; instead, the process occurs via filling the available adsorption space according to the mecha-

†To whom correspondence should be addressed.
E-mail: i.menshchikov@gmail.com

nism of volume filling of micropores described by Dubinin [19, 20]. Therefore, the scatter of points on the S_{BET}-methane storage capacity plots [5,15,16] can be attributed to the uncertainty of the BET method based on nitrogen adsorption data at 77 K or to the properties of activated carbon itself. So, the differences in adsorptive behavior of the ACs can be explained in terms of pore size distribution and surface chemical properties [21,22], which contribute to the energy of adsorbent-adsorbate interactions [23]. Chemical properties of carbon adsorbents are influenced by the nature of surface functional groups with heteroatoms, which, in turn, depend on a selected activation method (physical or chemical) and precursor from which the carbon is prepared. The choice of raw material to produce activated carbon is based on such considerations as [24]:

(i) relatively high yield of a high-quality product, which meets application requirements;

(ii) low content of inorganic matter;

(iii) availability and abundance of raw material.

In practice, inexpensive materials as biomass residue waste, coal, peat, and polymers are suitable precursors.

Conventional chemical and physical activation methods are used to produce activated carbons on an industrial scale. Extensive research work aimed at enhancing the porosity of the resulting AC adsorbent by using different activation conditions and activating agents was performed. For example, it was found that both CO_2 and steam used as an activating agent yielded activated carbons with a low density of functional groups [25]. However, CO_2 activation resulted in somewhat more stable oxygen-containing groups compared to steam [25]. Also, ACs prepared by CO_2 activation possess large micropore volume and narrow size distribution of micropores, whereas a micropore widening was a dominant effect of steam activation [26,27]. In [8], high surface activated carbon (HSAC) was made from microcrystalline cellulose pellets by CO_2 physical activation; the resulting product adsorbed approx. 147 m^3(STP)/m^3 at 3.5 MPa. Note that in 2012, the US Department of Energy (DOE) set the target deliverable capacity of a tank with adsorbent filled at the operating pressure of 3.5 MPa and ambient temperature to 263-264 m^3(STP)/m^3 [28]. The gravimetric adsorption capacity of the adsorbent must be 0.5 g/g [28]. The deliverable capacity is calculated as the amount of the gas (converted to the STP or NTP) that can be delivered from the ANG tank upon isothermal gas discharge with a pressure drop from the current level to a minimum value of pressure per unit of the tank [3,6].

Chemical activation has been widely used to produce highly microporous ACs at relatively low activation temperature. The use of KOH as an activating agent enhanced the specific surface area (higher than 900 m^2/s) and formation of oxygen-containing functional groups, although the yield was low [28]. The methane adsorption capacity of 12.8 mmol/g at 3.5 MPa was reported for AC microspheres prepared from starch by KOH chemical activation [29]. The authors attributed the superior adsorption performance to the high values of surface area and micropore volume, narrow pore size distribution, and low mesoporosity. The latter eases kinetics of methane adsorption/desorption [29]. A hybrid porous carbon was prepared by KOH microwave-assisted activation of coconut shell with polyetheretherketone, and the methane adsorption capacity of 9.7 and ~10 mmol/g was achieved at ambient and low temperatures (278 K) and 3.5 MPa [30]. Relatively low values of methane uptake of ~5 mmol/g were recorded for the peat-based steam activated carbon (Norit, Americas Inc.) at 298 K and 4 MPa [31].

In a large number of studies of methane/AC systems [3,6-8,32-37] a correlation between the methane adsorption capacity of AC and the structural and energy parameters introduced by the Dubinin theory of volume filling of micropores (TVFM) was shown [19,20]. The theory introduces three structural and energy parameters characterizing both the porous structure of an adsorbent and its adsorption behaviors: micropore volume W_0, average micropore half-width x_0, and characteristic energy of adsorption of a standard vapor (benzene) E_0. These parameters provide information averaged over many structural segments on the porous structure of real materials. However, in conjunction with the condition of temperature invariance of characteristic curves and coefficients of similarity, it is possible to calculate values of adsorption of gases and vapors in microporous adsorbents in a wide range of temperature and pressure [32-37]. The correlation mentioned above, however, is not straightforward; it is masked by influence of factors such as morphology, pore size distribution, presence, and density of functional groups, which are determined by a precursor and activation route, on methane adsorption [3,6-8]

In our work, we studied several series of activated carbons prepared from the raw materials that are widely used as AC precursors: coconut shells, peat, three types of polymers, silicon carbide, and mineral coal, using various activation routes. We compared experimental data on their porous structure, morphology, and chemical composition with the structural and energy parameters calculated by TVFM from standard adsorption isotherms. Such a comparison aims to establish a correlation between the adsorbents' physicochemical properties defined by the AC precursor types and activation method, and its methane adsorption performance in a wide pressure range. A comprehensive analysis of these data provides essential insight into the correctness of the theoretical description of the properties of real adsorbents. This is necessary for developing an approach for producing adsorbents with properties corresponding to theoretically optimal parameters for ANG storage systems.

EXPERIMENTAL

1. Samples

The most common raw materials for producing activated carbons are organic and inorganic carbonous materials based on vegetable feed [21,36-41], polymers [14,23,42-45], coals [14,42,43,46, 47], peat with different degree of metamorphism [14,48,49], and various carbides [50,51]. It is known [21-26,36-53] that the use of various raw materials (precursors) combined with different activation techniques allows adjusting physicochemical properties, morphology, porous structure, and surface chemistry of carbon adsorbents. Therefore, it seems appropriate to divide the studied carbon adsorbents into series according to the raw materials: C-series (vegetable feed - coconut shell), AR-V (mineral coal), T-series (peat), P-series (polymer feed), and AUK (silicon carbide material). Below we will briefly describe the conditions and procedures used for

Table 1. Structural and energy characteristics of carbon adsorbents prepared from various raw materials

Series	No.	Sample	Precursor[a]	Product[b]	Activation method[c]	E_0, kJ/mol	W_0, cm^3/g	x_0, nm	S_{BET}, m^2/g	W_S, cm^3/g	S_{me}, m^2/g	W_{me}, cm^3/g
P-series	1	P-10	PVDC	I	TD	30.0	0.47	0.40	972	0.47	-	-
	2	P-N	PFR	II	VGA	20.7	0.44	0.58	864	0.53	23	0.09
	3	P-300	Furfural			13.5	0.95	0.89	2,015	0.95	-	-
	4	P-3				18.7	0.50	0.64	980	0.80	41	0.30
	5	P-464				23.2	0.49	0.52	998	0.72	74	0.23
	6	P-5		III		21.2	0.53	0.57	1,093	0.88	391	0.35
T-ser.	7	T-3	Peat	IV	TCA+ WVA	16.9	0.50	0.71	962	0.63	78	0.13
	8	T-6				19.1	0.60	0.63	1,334	0.70	96	0.10
	9	T-4			TCA	20.6	0.48	0.58	957	0.72	105	0.24
C-series	10	C-1	Plant	V	WVA	19.7	0.62	0.61	1,111	0.62	-	-
	11	C-2				19.1	0.58	0.63	1,112	0.60	52	0.02
	12	C-7				23.9	0.40	0.50	790	0.42	31	0.02
	13	C-EC				24.7	0.34	0.49	665	0.34	-	-
-	14	AUK	SiC	VI	TCA	29.0	0.51	0.41	1,431	0.51	-	-
-	15	AR-V	Coal	IV	WVA	13.1	0.26	0.91	894	0.31	35	0.05

[a]PVDC - polyvinyl dichloride; PFR - phenol-formaldehyde resin.
[b]I - coarse particle powder; II - solid spherical grains of different fractions; III - solid spherical grains of monodisperse fraction; IV - extruded granules; V - ground fraction; VI - monolith rod.
[c]TD - thermal decomposition; VGA - vapor-gas activation; WVA - water vapor activation; TCA - thermochemical activation.
$W_s=W_0+W_{me}$ - specific total pore volume.

their preparation.

1-1. Carbon Adsorbents from Vegetable Feed (C-series)

The precursors widely used for the AC production are forestry and agricultural residues: biomass residue wastes with a high carbon content [40,42,52-58]. Due to low ash content, relatively cheap carbon adsorbents can be produced by steam activation without an additional washing step. The activation is generally carried out at elevated temperature between 1,023 and 1,373 K using oxidants such as steam, carbon dioxide, air, or their mixture [6,59,60]. In this study, we examined carbon adsorbents C-1, C-2, C-7, and C-EC (C-series, see Table 1, below), prepared in three stages including carbonization of crushed coconut shell at 870 K (1st stage), steam activation of a char thus obtained at 1,123-1,273 K (2nd stage), and subsequent size fractionation of the granular activated carbon (3rd stage). The samples differ in the activation duration (1h for C-7 and C-EC; 1.5 h for C-1 and C-2) and size fractionation into relatively small (0.7-1.2 mm for C-1), medium (0.9-2.4 mm for C-2) and large (1.3-3.0 mm for C-7 and 1.2-3.3 mm for C-EC) granules. As shown in [25,26], these variations in the synthesis conditions led to the differences in the burn-off degree calculated as percent weight loss upon activation and, consequently, in the porous structure of these ACs.

1-2. Carbon Adsorbent from Mineral Coal (AR-V)

The AR-V activated carbon is produced from mineral coal by preparing a paste from unoxidized lean and low-caking coals mixed with conditioned tree resin. The production process includes several stages: granulation through an extruding jet, drying the resulting granules in a drum furnace between 423 to 523 K, and preparation of a carbonized product in a rotary furnace at 773 to 873 K followed by the steam activation step at 1,123 to 1,253 K. The process of the synthesis is described in detail in [42].

1-3. Peat-derived Carbon Adsorbents (T-series)

Shredded and dehydrated peats with a high level of decomposition or their mixtures were used as raw materials to prepare the T-series of carbon adsorbents. After crushing and separation, the raw material was permeated with K_2S and mixed to form a homogeneous elastic paste. This preform was pressed and granulated using extruding jets. The cylindrical granules thus obtained were dried and carbonized in a drum furnace by flue gases to remove both the residual moisture and volatile compounds and decompose the peat organic constituent. The carbonized granules were activated in a rotary furnace at 1,053-1,133 K. The activated granules can contain up to 30 wt% potassium, 10% sulfur, and up to 10 wt% ash components inherited from peat [48]. The activated granules were cooled and passed through a set of washing procedures, including leaching by alkali solutions, washing in water and hot hydrochloric acid, and final rinsing with water to remove the impurities. In the end, the wet granules were placed into a tumble drier and then into a pre-heat furnace to reduce the moisture content down to 3-5 wt%. The additional steam activation step in the furnace gave rise to a developed porosity of the resulted peat-based activated carbons [42,48,49].

1-4. Carbon Adsorbents from Polymers (P-series)

The adsorbents of the P-series were prepared from thermo-reactive linear (P-10) and cross-linked (P-N) polymers, and polymer blends (P-3, P-5, P-464, and P-300).

The P-10 adsorbent was prepared by thermal decomposition of polyvinyl dichloride (PVDC) under a nitrogen atmosphere at temperatures from 800 to 1,000 K as a result of the following reaction [61]:

$$(C_2H_2Cl_2)_n \rightarrow 2n\mathrm{HCl} + 2n\mathrm{C} \quad (1)$$

Due to the instantaneous solidification of the final product, the pyrolysis of PVDC proceeds via a solid-phase mechanism without the formation of mesophases, which is typical for many linear thermo-reactive polymers (polyvinyl chloride, polystyrene). It was found [42] that a developed porous structure in the PVDC-derived carbon was formed entirely at the pyrolysis temperature from 773 to 873 K when up to 95% HCl is released. A further increase in the pyrolysis temperature leads to a significant reduction of the porosity.

The P-3, P-5, P-464, and P-300 samples were prepared by liquid molding of thermo-reactive furfural copolymer with epoxy resin, which was proposed as a precursor for producing activated carbons, for example, in [42]. The granules were subjected to two-step carbonization in a furnace at 723-773 K and 1,073-1,123 K followed by physical activation in the hermetically sealed chambers. The samples were activated using steam and carbon dioxide at 1,123 K. By changing the duration of the carbonization or activation stages, it was possible to prepare the adsorbents differing in degree of carbon burn-off and porous structure.

The P-N adsorbent was prepared from cross-linked thermo-reactive polymer - phenol-formaldehyde resin. The two-step carbonization of polymer samples was carried out first in a rotary drum of an electrically heated retort-type oven (first step) and then in a stationary furnace in a carbon dioxide atmosphere; the temperature was varied from 573 to 1,073 K. After the carbonization, the product was activated by steam and carbon dioxide at 1,173 K.

Carbonization of thermo-reactive carbonaceous materials includes four stages proceeding at gradually increasing temperatures from 573 to 3,573 K, which results in a progressive increase in the amount of ordered graphite phase [14]. In our case, the carbonization of the samples prepared from furfural and phenol-formaldehyde resin was completed at 1,273 K, which corresponds to the first two stages of carbonization characterized by the formation of only small clusters of ordered carbon. Therefore, we assumed that the structure of these adsorbents was characterized by a significant amount of a disordered carbon phase.

1-5. Carbon Adsorbent Prepared from Silicon Carbide (AUK)

The AUK carbon adsorbent was made from hexagonal silicon carbide (α-SiC) by thermochemical leaching of Si atoms in a Cl_2 flow at 1,273 K:

$$\mathrm{SiC} + 2\mathrm{Cl_2} \xrightarrow{1{,}173\ \mathrm{K}} \mathrm{SiCl_4} + \mathrm{C} \quad (2)$$

This thermochemical reaction produces volatile $SiCl_4$ gas evacuated from the reaction zone. As a result, a rigid carbon matrix with a uniform network of micropores is formed [62-64].

1-6. Adsorptive

The adsorbate used was reagent grade methane (99.98%). The following values were used in calculations: molecular mass M= 16.0426 g/mol, boiling point T_0=111.66 K, critical temperature T_{cr}= 190.77 K, and critical pressure p_{cr}=4.641 MPa [65].

2. Methods

2-1. X-ray Powder Diffraction, Small-angle X-ray Scattering, Scanning Electron Microscopy

Small-angle x-ray scattering (SAXS) and x-ray diffraction (XRD) provide complementary information. In essence, the diffraction patterns are mostly determined by (relatively) ordered crystallites and their mutual arrangement. In contrast, the scattering of x-rays is dependent on the contrast of electronic density and (in isotropic case) is not sensitive to the spatial arrangement of domains [66-68].

XRD was used to examine the phase composition of the carbon adsorbents. XRD patterns were recorded using an Empyrean (Panalytical BV) diffractometer in the Bragg-Brentano geometry using Ni-filtered CuKα-radiation (λ_{Cu}=0.1542 nm) in the 2θ angular range of 10-120°. The samples were ground to a powder; no binder was employed. ICDD PDF2 database was used for phase identification.

The porous structure of the carbon adsorbents was examined using SAXS at a SAXSess diffractometer (Anton Paar). Powdered samples were measured in transmission geometry in a vacuum chamber. Monochromatic Cu-Kα radiation and 2D Imaging Plate detector were employed, the range of scattering q vectors from 0.1 to 27 nm^{-1}. Characteristic micropore sizes of the carbon adsorbents were evaluated using Guinier approximation [69].

The surface morphology and elemental chemical composition of the mechanically ground AC samples were investigated by scanning electron microscopy (SEM) using Quanta 650 FEG scanning electron microscope (FEI, United States), equipped with an Oxford energy dispersive X-ray (EDX) detector. Both the roughness and high porosity of the AC samples lead to significant errors in the percentage of an element. However, the SEM-EDX data allowed us to carry out a semi-quantitative comparison of the studied samples by chemical composition.

2-2. Adsorption Experiments and Evaluation of Structural and Energy Characteristics of Carbon Adsorbents

SEC values such as specific micropore volume W_0, characteristic energy of adsorption of standard benzene vapor E_0, and effective half-width of micropores x_0 were calculated for the AC adsorbents from the standard benzene vapor adsorption data for at 293 K measured on a Quantachrome Autosorb iQ multifunctional surface area analyzer using the Dubinin-Radushkevich (D-R) equation [19,20]. The Brunauer-Emmet-Teller (BET) equation was used to determine the specific surface area S_{BET} from the nitrogen adsorption data at 77 K [17,18].

Methane adsorption equilibria on the AC samples were measured in a wide range of pressure from 0.1 to 10 MPa and at 303 K by the volumetric-gravimetric method using three original adsorption devices developed in IPCE RAS and described in detail in our previous works [70-72]:

- a semi-automatic adsorption weight vacuum unit (from 5 Pa to 0.1 MPa, gravimetric method; accuracy of ±1.5%) [70];
- a universal adsorption-dilatometer setup (0.1-6 MPa, volumetric method, accuracy of ±3%) [71];

• an original volumetric-gravimetric high-pressure set-up (0.2-10 MPa, accuracy ±5%) [72].

The equilibrium values of absolute methane adsorption were calculated from experimentally measured parameters of an adsorption system as:

$$a = \frac{N - (V - V_{ads})\delta_{gas}(P, T)}{m_0}, \text{ where } V_{ads} = V_{He} + m_0 W_0. \quad (3)$$

Here, N is the total amount of gas introduced into a system, [mmol]; V is the total geometric volume of the system, [cm^3]; V_{ads} is the volume of an adsorbent with micropores, [cm^3]; δ_{gas} is the density of a gaseous phase, [mmol/cm^3]; m_0 is the mass of a regenerated adsorbent, [g]; V_{He} is the volume of the adsorbent determined via helium pycnometry, [cm^3].

RESULTS AND DISCUSSION

1. Structural and Energy Characteristics of Carbon Adsorbents

TVFM is a reliable tool for analyzing methane adsorption in carbon adsorbents in a wide *PT*-range [31-35,70-74]. The most general formula of TVFM known as the Dubinin-Astakhov equation [19,20] is as follows:

$$a = a_0 \exp[-(A/E)^n] \quad (4)$$

where A=RT ln (P_S/P) [kJ/mol] is the differential molar work of adsorption; a_0 [mmol/g] is the limiting value of adsorption at the temperature T [K], which depends on the specific volume of micropores W_0 [cm^3/g]; E [kJ/mol] is the characteristic energy of gas adsorption; parameter *n* is determined by surface chemistry and degree of uniformity of porous structure of an adsorbent. Eq. (4) with *n*~2 is commonly used to describe the adsorption properties of carbon adsorbents (D-R equation); in the case of zeolites: *n*~3. In the present work, the structural and energy characteristics (SEC) of the carbon adsorbents were evaluated using the D-R equation. As follows from TVFM and Eq. (4), the amount of adsorbed gas depends on two key parameters: E and W_0. For a model of slit-like pores, the characteristic energy of adsorption is related to the effective half-width of micropores by a formula: $E=12\beta/x_0$, where β is the coefficient of similarity for the gas under study. The value of β is evaluated relative to the standard benzene vapor: $\beta=E/E_0$.

In practice, it is hard to achieve a simultaneous increase in the values of E and W_0 of an adsorbent that would maximize the value of gas adsorption. Indeed, the activation process aimed at developing the porous structure of activated carbons implies an increase in the volume and radius of micropores. At the same time, the expansion of the pores decreases E. However, the high characteristic energy of adsorption onto a carbon adsorbent with narrow micropores provides considerable adsorption at low pressures [64]. On the other hand, high values of micropore volume are required for high adsorption capacity.

Figs. 1 and 2 show the isotherms of adsorption of standard benzene vapors onto the studied carbon adsorbents measured at 293 K. The initial sharp rise of the adsorption isotherm was followed by a plateau, and the SEC values evaluated by applying the D-R equation (see Table 1) indicate a well-developed microporous structure. A hysteresis loop is observed in adsorption isotherms for some

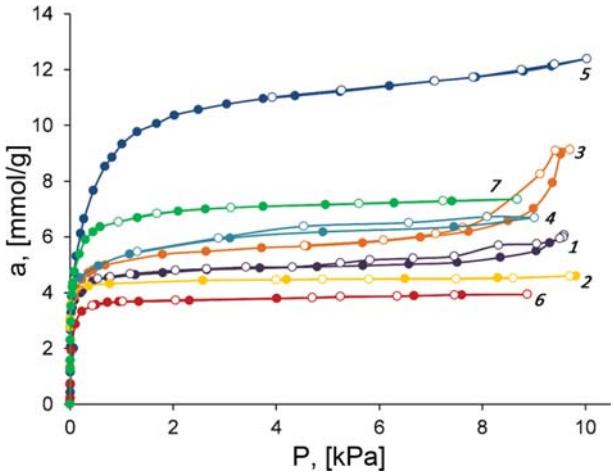

Fig. 1. The isotherms of benzene vapor adsorption (filled symbols)/ desorption (open symbols) on the AC samples of P-series: P-N (*1*), P-10 (*2*), P-3 (*3*), P-5 (*4*), and P-300 (*5*) and C-series: C-EC (*6*), C-1 (*7*) at 293 K.

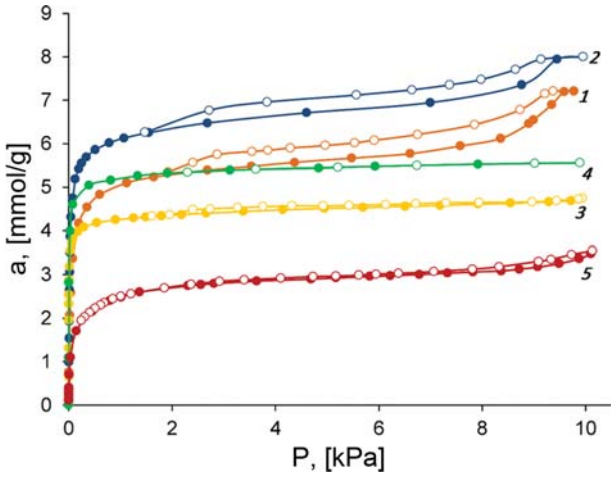

Fig. 2. The isotherms of benzene vapor adsorption (filled symbols)/ desorption (open symbols) on the carbon adsorbents: T-3 (*1*), T-6 (*2*), C-7 (*3*), AUK (*4*), and AR-V (*5*) at 293 K.

adsorbents of the P-series (P-3, P-5, and P-N), T-series, AR-V, and C-7, which is indicative of a presence of mesopores with specific surface area S_{me} [m^2/g] and volume W_{me} [cm^3/g] determined by the BJH method [75]. The highest adsorption of benzene vapors was found for the P-300 and T-6 adsorbents prepared from polymer and peat, respectively (Figs. 1 and 2). As follows from Table 1, these adsorbents possess the highest values of BET specific surface areas: S_{BET} (P-300)=2,015 m^2/g and S_{BET} (T-6)=1,334 m^2/g, but no correlation between the value of benzene vapor adsorption and volume of micropores or characteristic energy is observed.

Table 1 demonstrates a difference between the SEC values determined for the studied carbon adsorbents, which undoubtedly reflects differences in their porous structure. The P-10, AUK, C-1, C-2, C-7, and C-EC adsorbents are mostly microporous, whereas the porous structures of the carbons, which were prepared from furfural, PFR, and peat, include a significant amount of mesopores. In any

case, the studied AC samples have relatively high values of micropore volume and BET surface. As follows from Fig. 1, the micropores sizes, $2x_0$, ranging from 0.8 to 1.8 nm, provide a high density of adsorbed methane. Therefore, we can consider all studied activated carbons as effective adsorbents for the ANG system within a wide range of pressure and temperature. According to Table 1, the samples P-300 and T-6 are the most promising adsorbents, possessing not only the highest BET surface but also relatively significant micropore volume. Moreover, there are no mesopores in P-300.

However, the SEC data are not sufficient for a comprehensive characterization of real activated carbons targeted at their applica-

Table 2. The elemental composition of ACs prepared from various precursors (at%)

Element	P-series						C-series				T-series				
	P-3	P-5	P-464	P-300	P-10	PN	C-EC	C-7	C-2	C-1	T-3	T-4	T-6	AUK	AR-V
C	96.2	96.7	96.7	96.1	91.0	95.0	92.0	96.0	93.0	92.0	75.6	81.6	71.5	96.0	90.7
O	3.5	3.2	2.7	3.7	7.2	5.0	6.9	3.5	6.5	6.0	18.3	14.7	21.0	3.2	6.3
K	-	-	-	-	-	-	1.1	0.5	0.5	2.0	0.2	0.3	0.2	-	-
S	0.3	0.1	0.6	0.2	-	-	-	-	-	-	0.7	1.2	0.7	-	0.1
Si	-	-	-	-	-	-	-	-	-	-	2.9	1.1	5.2	0.5	1.3
Al	-	-	-		-	-	-	-	-	-	1.9	0.3	0.7	-	1.1
Cl	-	-	-	-	1.3	-	-	-	-	-	-	0.2	0.2	0.3	-
Ca	-	-	-	-	-	-	-	-	-	-	0.2	0.5	0.5	-	0.3
Fe	-	-	-	-	0.5	-	-	-	-	-	0.2	0.1	-	-	0.2

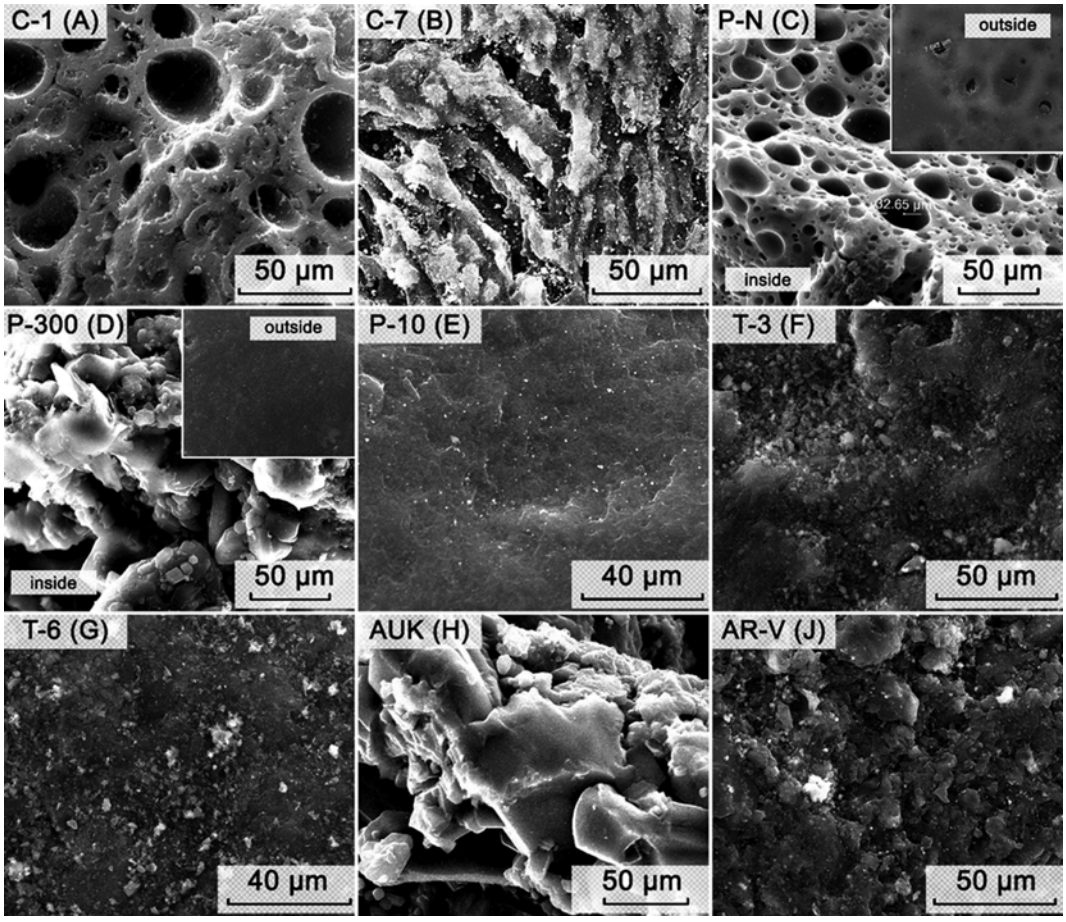

Fig. 3. SEM images of the surface of the adsorbents derived from coconut shell: C-1 (A) and C-7 (B), phenol-formaldehyde resin: P-N (C), furfural: P-300 (D), PVDC: P-10 (E), peat: T-3 (F) and T-6 (G), silicon carbide: AUK (H), and mineral coal: AR-V (J). The inset is a selected area of SEM image of the outer surface of the P-N and P-300 granules.

tion in the ANG system. Additional information on factors affecting the adsorption behaviors of activated carbons, such as morphology and surface chemistry, can be obtained from XRD, SAXS, and SEM.

2. Elemental Chemical Composition and Surface Morphology

2-1. Elemental Chemical Analysis

Table 2 summarizes the elemental composition of the carbon adsorbents as determined from the SEM-EDX data.

The main constituents of the AC samples are carbon and oxygen (see Table 2). Heteroatoms (Al, Si, Cl, Ca, Fe) are partly inherited from the raw materials (peat, mineral coal) and chemicals (e.g., K_2S) used in the activation procedure. The composition of coconut shell is responsible for the traces of K in the adsorbents of C-series. Some heteroatoms are retained in non-carbonaceous mineral grains such as quartz and feldspars, common in peat and coal phases.

The T-6 sample with the highest degree of activation contains the lowest carbon content and the highest number of heteroatoms, including S and Cl, which remain after activation. These elements can act as efficient adsorption centers explaining the high value of the characteristic energy of adsorption (see Table 1). The high degree of activation implies that this adsorbent possesses a significant volume of micropores (see Table 1). A combination of these factors is likely a prerequisite for a high adsorption efficiency of the ANG systems based on T-6.

2-2. SEM Analysis of Surface Morphology

Figs. 3 and 4 show the images obtained for the studied carbon adsorbents at various magnifications. At the scales of 40 to 100

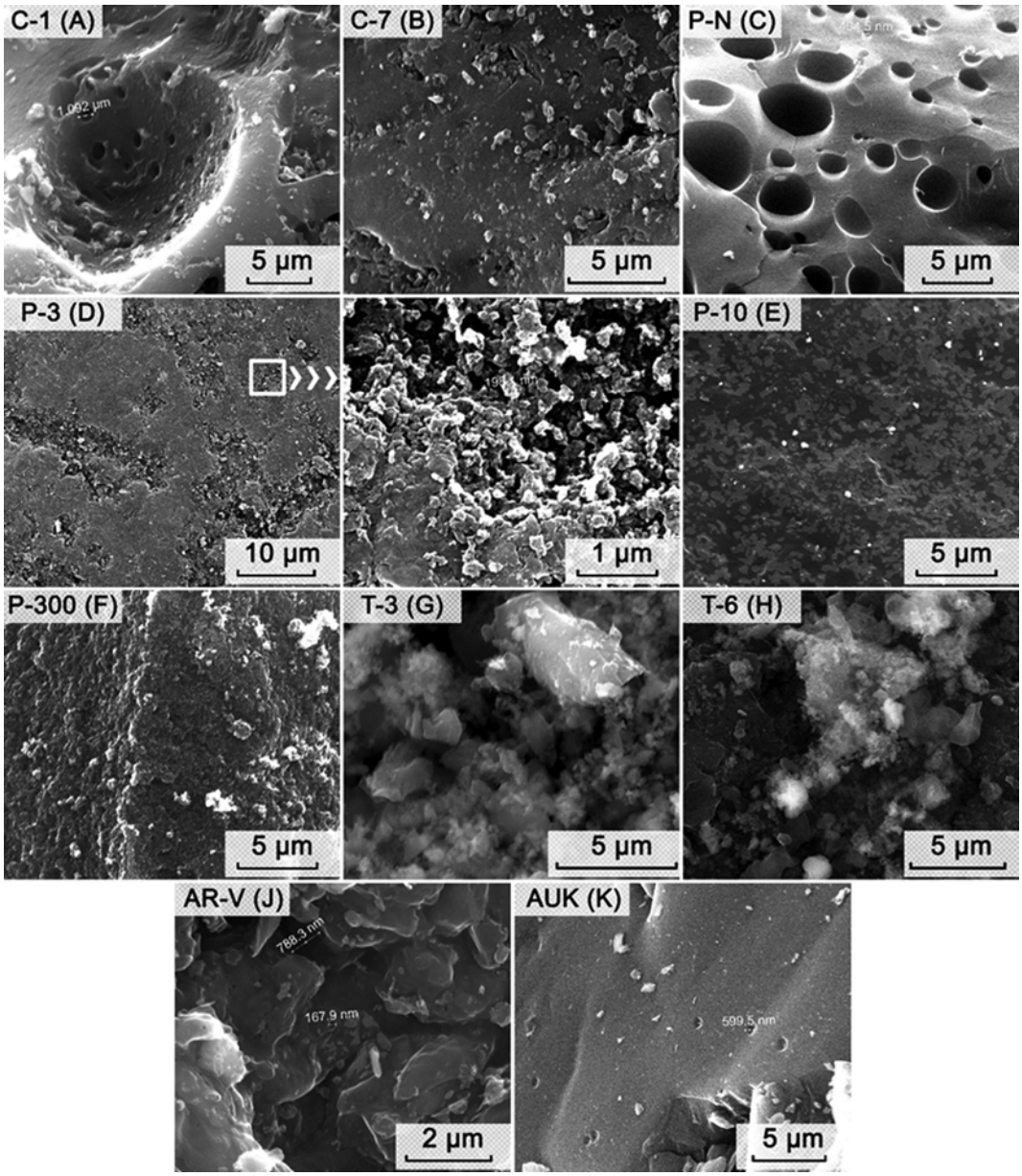

Fig. 4. SEM images of the surface of the AC samples derived from coconut shell: C-1 (A) and C-7 (B), phenol-formaldehyde resin: P-N (C), furfural: P-3 (D) and P-300 (F), PVDC: P-10 (E), peat: T-3 (G) and T-6 (H), mineral coal AR-V (J), and silicon carbide AUK (K).

μm, the dependence of morphology on the type of AC precursor and activation procedure becomes apparent. In particular, the C-1 sample with the highest activation degree possesses large cylindrical transport pores with a diameter of 30-40 μm perpendicular to the surface (Fig. 3(A)). At the same time, the less-activated C-7 sample looks completely different (Fig. 3(B)): it consists of domains 100×100…200 μm in size composed by identically oriented 20×50…70 μm carbon structures. Fig. 3(C) shows a cheese-like surface of the P-N sample covered by cylindrical transport pores ~20-30 μm in diameter. The outer surface of P-N granules is sufficiently smooth between the pore outcrops. The P-300 granules from furfural also possess a smooth and even outer surface without noticeable defects. However, the cleavage surface of the P-300 granule (inside) is composed of round structures and irregular macropores ~50 μm in size (Fig. 3(D)). Among the studied activated carbons, P-10 derived from PVDC has the most homogeneous and dense surface covered by large transport pores (Fig. 3(E)). The flake shape of the T-3 and T-6 particles is determined by morphological features of peat (Fig. 3(F) and (G)); no wide macropores were observed that is indicative of a high density of carbon material. Fig. 3(H) shows the rough surface of AUK covered by irregular transport pores less than 100 μm in size. The irregular transport pores smaller than 10-20 μm are randomly distributed over the granular surface of AR-V (Fig. 3(J)).

The images obtained at higher magnifications also confirm the dependence of the carbon surface morphology on the precursor material (Figs. 4(A)-(K)).

The influence of the burn-off degree on the AC morphology is illustrated by the samples of C-series derived from the same raw material - coconut shell, but differing in the degree of activation: C-1 and C-7 (Figs. 4(A) and (B)). Unlike the rough surface with small inclusions and pores less than 0.5 μm in size in C-7, the C-1 carbon adsorbent with a higher activation degree shows a relatively smooth surface with the cylindrical transport pores ~1 μm in diameter and narrower (<0.5 μm) pores. The use of different precursors explains the dissimilar images obtained for the P-N, P-3 (or P-300), and P-10 samples. Indeed, the structure of the PVDC-based carbon (P-10) (Fig. 4(E)) is noticeably denser compared to that of the carbons from furfural (P-3 and P-300, see Fig. 4(D)) and PFR (P-N, see Fig. 4(C)); its surface is uniform at low-to-moderate magnification. The P-N sample is the only one with visible transport pores ~5 μm in diameter. At moderate magnification, the P-3 and P-300 samples show granular featureless surfaces with small (<1 μm) pores (Figs. 4(D) and (F)). At higher magnification,

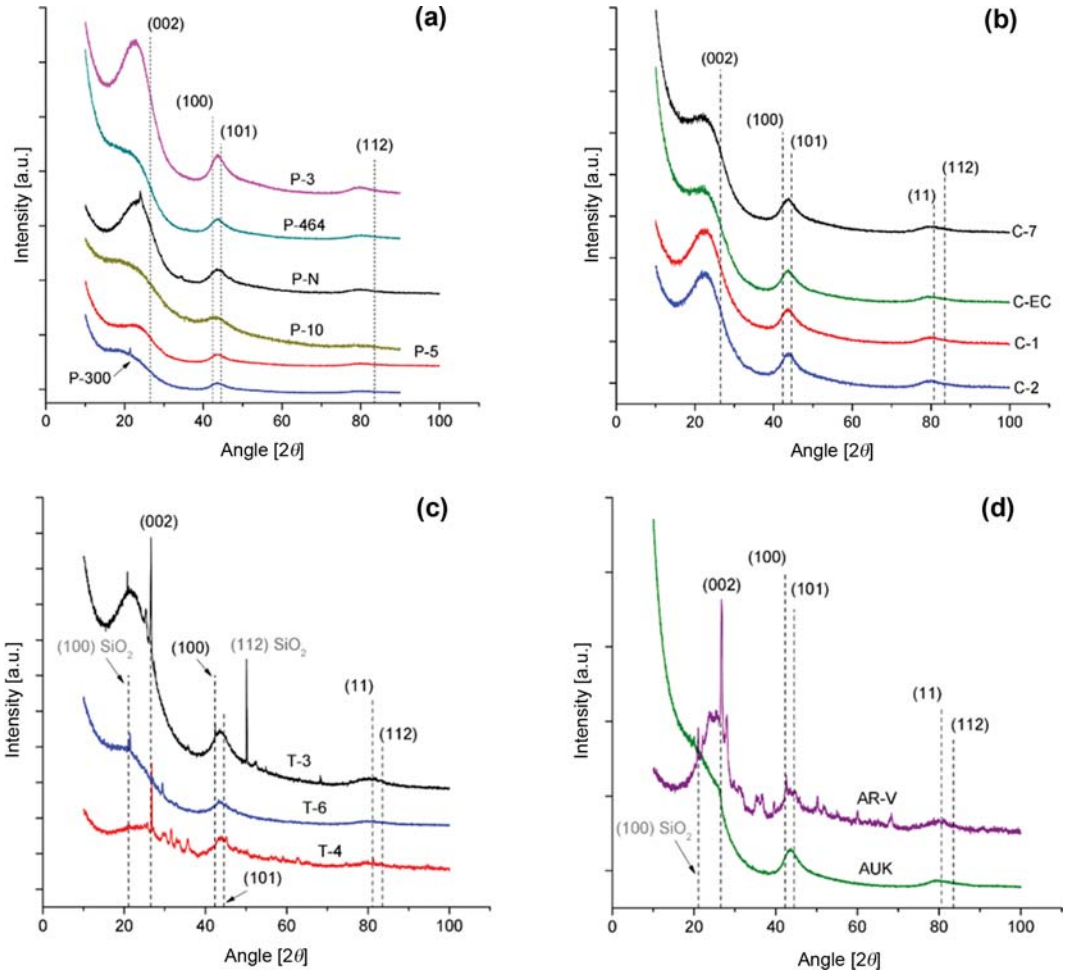

Fig. 5. XRD patterns for activated carbons prepared from polymers (a), coconut shells (b), peat (c), silicon carbide AUK and mineral coal (d). Dashed lines show the main reflections of graphite and quartz.

the P-3 sample appears rough: it is composed of ~0.2 μm carbon fragments separated by 0.1-1 μm macropores. The SEM images for T-3 and T-6 (Figs. 4(G) and (H), respectively) display a heterogeneous granular surface and visible open pores with a diameter no more than 2-10 μm. Fig. 4(J) for AR-V demonstrates crystal-like structure 1-2 μm in size separated by a developed system of macropores with a size of ~0.8 μm. SEM reveals that P-3, P-300, and AUK possess the densest structure with an insignificant amount of macropores (Figs. 4(E), (F), and (K)). The AUK sample has the smoothest surface, which is similar to a chip of a crystal and its porous structure consists mainly of micro- and ultramicropores.

When analyzing the morphological features of the samples, it should be emphasized that *ceteris paribus*, carbon adsorbents with an insignificant (or zero) macropore volume fraction would be characterized by a higher adsorption activity relative to vapors and gases, including methane, thereby providing a considerable adsorption capacity of the ANG system.

3. X-ray Measurements

3-1. Phase Composition by XRD Measurements

Figs. 5(a)-(d) show the XRD patterns for each AC series according to the type of precursor. The diffraction patterns show that all the samples are represented by graphitic carbon; occasionally, other crystalline impurities (mostly quartz and albites) are also observed. Leaving aside the impurities, one can distinguish two large groups of the XRD patterns that differ from each other in the degree of order of the graphitic phase and fraction of the ordered phase. The difference can be illustrated with an example of the P-series (Fig. 5(a)). The diffraction patterns of P-N and P-3 show a set of relatively strong, albeit broad peaks, which are attributed to relatively abundant well-ordered carbon crystallites with somewhat higher interlayer spacings than in ideal graphite. We note that, as shown in [76,77], when the graphitic crystallites become smaller than 2-3 nm, the width and position of the 002 diffraction peak cannot be used for reliable determination of size and lattice spacing because of their strong influence on the detailed structure and morphology of the graphene layer stacks and surface termination. All other samples from this series possess a very intensive scattering background due to the amorphous component and poorly formed graphitic peaks with low intensity.

Therefore, in terms of diffraction, the P-N and P-3 samples could be described as relatively large (about 1-2 nm) graphite-like crystallites embedded into an amorphous matrix. In other samples, the amount of nanocrystals is much less. Similar conclusions could be made for the carbon adsorbents from another series. By summing these facts, we can conclude that the P-N, P-3, C-1, C-2, T-3, and AR-V samples belong to the first group, i.e., their structure can be identified as "nanocrystallites in the amorphous matrix." In the T-3, T-4, and AR-V samples, the strong peaks of well-formed graphite are observed. These graphite crystallites are likely inherited from the precursors of these adsorbents - peat and coal, with a high degree of thermal metamorphism. The activation process and heating stages promoted their ordering and growth.

3-2. Analysis of SAXS Data for Carbon Adsorbents

The SAXS method provides subatomic structural information in the resolution range from several angstroms to hundreds of nanometers by analyzing the scattering intensity I expressed as a function of the scattering vector $q=4\pi\cdot\sin(\theta)/\lambda$ [1/nm] In general terms, the exponent n in the dependence $I\sim q^n$, or, when representing it in the logarithmic coordinates, a slope of the linear function $\log(I)\sim n\cdot\log(q)$ is sensitive to the morphology of a sample. Inflection points allow the determination of characteristic sizes of structural heterogeneities responsible for the scattering [66-68].

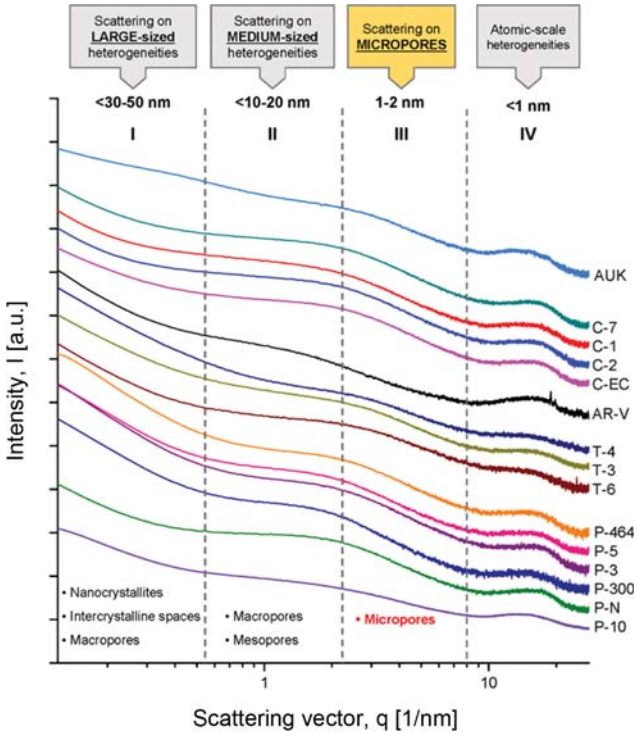

Fig. 6. Log-log plot of intensities versus scattering vector for carbon adsorbents prepared from various raw materials.

The linearity of the Guinier plots in the region between ~2-8 nm^{-1} (marked as III in Fig. 6) indicates x-ray scattering by a monodisperse system. This fact allows one to calculate an important parameter of the porous structure of carbon adsorbents - radius of gyration of micropores R_G [66-68]. The Guinier formula [69] can be written in a linear form

$$\ln I=\ln I_0-k(q^2R_G^2), \quad (5)$$

where k is the coefficient determined by a geometry of pores. When considering slit-like and cylindrical pore models, which are the best approximation to real pores in carbon adsorbents in terms of the mechanism of their formation, the values of k are 1 and 1.2, respectively. The radius of gyration of the cross-section of a cylindrical pore with infinite length, R_{GC}, can be calculated as:

$$q^2I(q)=I_0\cdot\exp[-R_{GC}^2q^2/2]. \quad (6)$$

In the case of a slit-like pore, R_{GS} is:

$$q^2I(q)=I_0\cdot\exp[-R_{GS}^2q^2]. \quad (7)$$

The average sizes of cylindrical and slit-like model pores, radius R_T and width H_S, can be determined from the following relationships:

$$R_T = 2^{1/2} R_{GC}, \quad (8a)$$

$$H_S = 3^{1/2} R_{GS}. \quad (8b)$$

Dubinin with coworkers [78] suggested that for carbon adsorbents with relatively homogeneous chemical composition and narrow slit-like pore size distribution, the following relationships between SEC and R_G should be fulfilled:

$$R_G = K \cdot x_0 \approx x_0 \sqrt{\left(\frac{\gamma^2}{2} + \frac{1}{3}\right)}, \quad (9)$$

where K is the coefficient of proportionality determined by a ratio between crystallite radius r to the half-width of micropore, $\gamma = r/x_0$, and can be calculated from an empirical relationship:

$$E_0 R_G = 14.8 \pm 0.6 \text{ [kJ·nm/mol]}. \quad (10)$$

As long as the parameter γ is constant and Eq. (10) is valid, K= 1.23. Therefore, the ratio between R_G and x_0 was derived from Eqs. (9) and (10):

$$R_G = (1.23 \pm 0.05)\, x_0 \text{ [nm]}, \quad (11)$$

Fig. 7 shows the dependences of parameters R_G, R_T, and H_S on the average half-width of micropores for all carbon adsorbents under study (a), and separately for the samples of P-series (b), C-series (c), and T-series (d). The data for AR-V and AUK are shown only in Fig. 7(a).

The relative deviation of the SAXS data for most samples of the C- and P-series from the linear function (11) is within an interval of ~20%. Therefore, one can conclude that the structure of these adsorbents is close to that of AC with homogeneous chemical composition. Whereas, the more significant deviation from Eq. (11) observed for other adsorbents can be attributed to the specific features of their crystal structure, porous system, and chemical composition, which were revealed by XRD and SEM:

i. Fluctuations of the values of r/x_0 ratio in the volume of carbon sample associated with significant heterogeneity of the phase composition of this material, which determines a diverse range of pore shapes and sizes. As an example, P-300 exhibits a high degree of amorphism, as evidenced by the XRD data. Another example is P-10, whose micropores cannot be described by the models of pore geometry (see Fig. 7(b))

ii. Heterogeneous chemical composition of carbon adsorbents determined by the presence of heteroatoms, which were found for the samples of T-series (Fig. 7(d)) and AR-V (Fig. 7(a)) in the XRD and SEM experiments.

Considering the entire set of the samples, one cannot establish a single function adequately describing a correlation between R_G determined from the SAXS data and x_0 inferred from the benzene adsorption data via TVFM, although, in general, R_G increases with

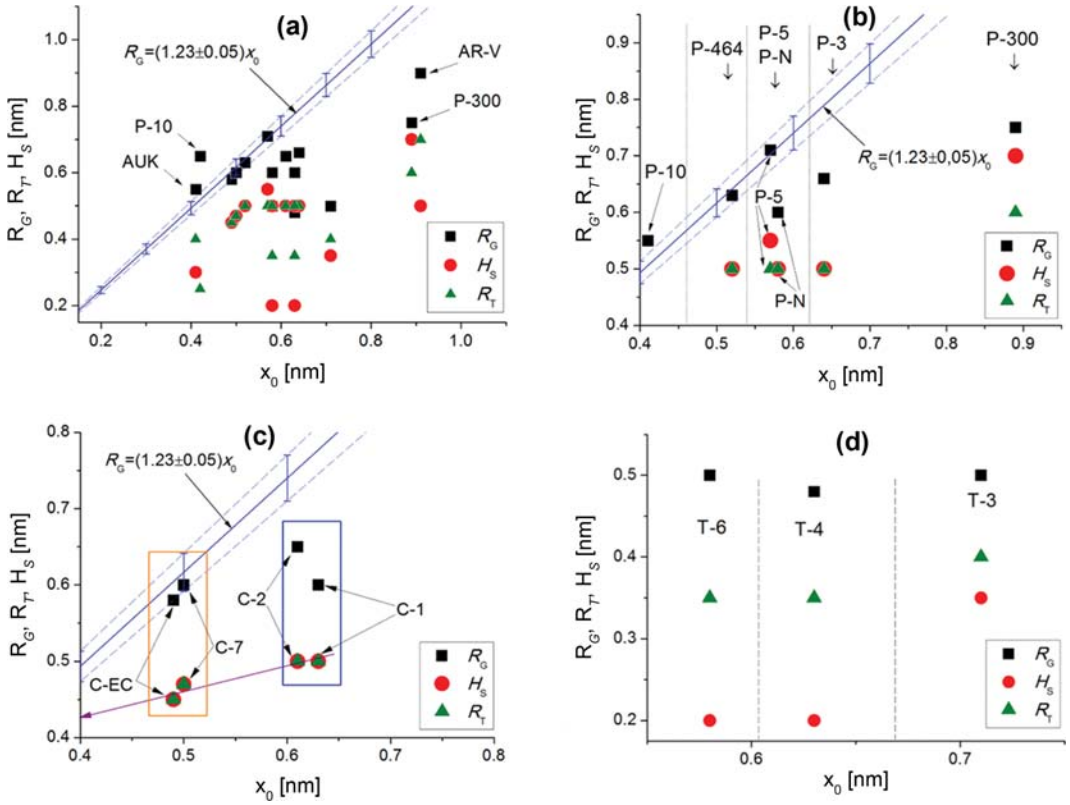

Fig. 7. Correlation between the values of model micropores calculated from the SAXS experiments for all studied carbon adsorbents (a), adsorbents of P-series (b), C-series (c), and T-series (d): Radius of gyration R_G (■), radius of cylindrical pore R_T (▲), width of slit-like pore H_S (●), and average half-width x_0, calculated using TVFM. The straight line on A, B, and C corresponds to a linear relationship (9) at K=1.23; the straight line with an arrow in (c) is a result of a linear fit of parameters determined from SAXS: R_T and H_S. The dotted lines in (a), (b), (c) indicate limits of validity of Eq. (11).

x_0 (see Fig. 7(a)). A similar trend was established for dependences $R_T(x_0)$ and $H_S(x_0)$.

However, the analysis of particular data sets grouped by precursor type (Fig. 7(b)-(d)) makes it possible to distinguish the specific relationships for each series of carbon adsorbents. Namely, for the C-type samples, the dependency of R_T and H_S on x_0 can be approximated by a straight line (Fig. 7(c)). The fit line does not pass through the origin. A similar shift from the 1 : 1 correlation of R_G and x_0 was earlier reported by Shiryaev et al. [68] and likely results from very different formalisms employed for evaluating these parameters from the X-ray scattering and adsorption data.

Table 3 summarizes the values of product $E_0 \cdot R_G$ evaluated from the data on standard benzene vapor adsorption (E_0) and SAXS (R_G) for the studied carbon adsorbents prepared from various raw materials.

As follows from Table 3, the average value of 12.8 kJ·nm/mol for $E_0 \cdot R_G$ over the entire set of the studied samples differs from that reported by Dubinin and Plavnik [78]. However, this product does broadly depend on the precursor. For example, the average values of $E_0 \cdot R_G$ for the adsorbents of P- and C-series, 13.8 and 13.2 kJ·nm/mol, are close to that in Eq. (10). According to the XRD data, these adsorbents are composed primarily of highly disordered carbon. Following this logic, we might expect that a significant deviation of the obtained values of $E_0 \cdot R_G$ from that in Eq. (11) is observed for the adsorbents of T-series and AR-V. This deviation is an indicator of a high degree of chemical heterogeneity determined by the presence of a large number of heteroatoms (see Table 2) and special features of the porous structure formed as a result of chemical activation (TCA+WVA or WVA). But note that for the adsorbents with heterogeneous surface composition, the deviation from Eqs. (10) and (11) increases with increasing micropore volume of these adsorbents due to a more significant contribution of chemical impurities to adsorption processes. Thus, it is necessary to consider both the geometrical parameters of the porous system, which are significantly influenced by carbonization and activation conditions and surface chemistry, which is inherited from a precursor material and largely determines the energy of adsorbate-adsorbent interactions.

Summarizing the above data, we assume that P-300 and T-6 ($E_0 \cdot R_G$=10.1 and 9.1 kJ·nm/mol, respectively) exhibit a high methane adsorption capacity. Indeed, the high adsorption capacity of P-300 is determined by the high degree of activation (implying a well-developed porosity with a significant micropore volume) achieved through the VGA process. While the expected high adsorption behaviors of T-6 can be attributed to the heterogeneous chemical composition caused both by the precursor and the specific features of the pore formation upon TCA. Thus, different AC adsorbents can have pores of identical configuration and sizes, as evidenced by SAXS, but when analyzing their adsorption behaviors, it is necessary to take into account the influence of surface chemistry on the characteristic energy of adsorption E_0.

Table 3. The values of product $E_0 \cdot R_G$ evaluated from both the adsorption and SAXS data for carbon adsorbents prepared from various precursor materials

Sample	Precursor	R_G, nm	$E_0 \cdot R_G$, kJ·nm/mol		
P-10	Polymer	0.65	18.6	13.8*	12.8**
P-N		0.60	12.4		
P-300		0.75	10.1		
P-3		0.66	12.4		
P-464		0.63	14.5		
P-5		0.71	14.9		
T-3	Peat	0.50	8.5	9.3*	
T-6		0.48	9.1		
T-4		0.50	10.3		
C-1	Plant	0.65	12.8	13.2*	
C-2		0.60	11.2		
C-7		0.60	14.4		
C-EC		0.58	14.2		
AUK	SiC	0.55	16.1	-	
AR-V	Coal	0.90	11.9	-	

*Averaged over one series

**Averaged over the entire set of adsorbents

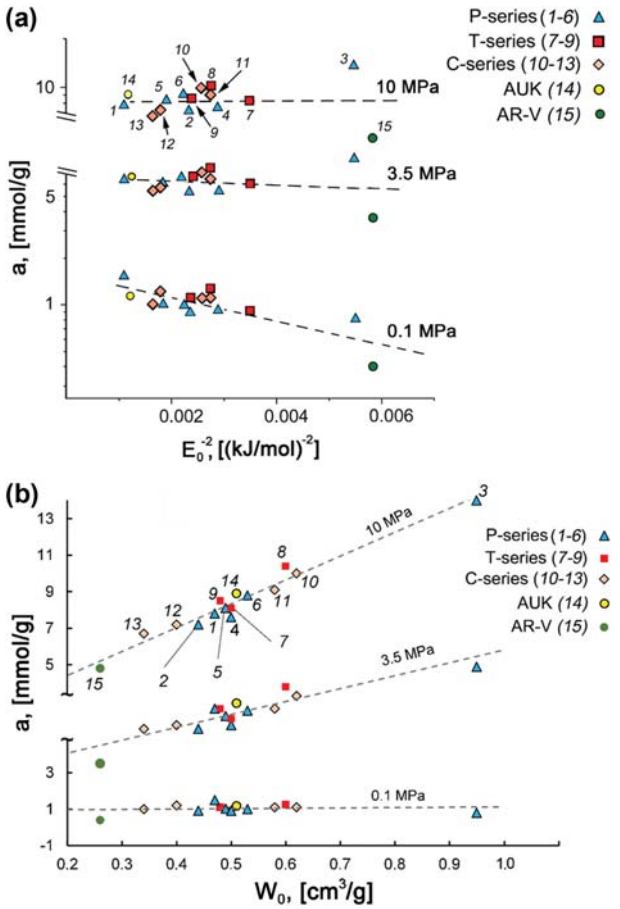

Fig. 8. Methane adsorption capacity in the studied AC series at T= 303 K and P=0.1, 3.5, and 10 MPa versus basic TVFM parameters: characteristic energy of adsorption (a) and micropore volume (b), in coordinates of the D-R equation (Eq. (4)). Symbols are numbered in the same order as the samples in Table 1. The dashed lines are the linear approximation.

4. Methane Adsorption

In our recent works, we reported the data on methane adsorption in the studied carbon adsorbents measured between 178-333 K within a wide range of pressures [9,33-35,64,70,71,73]. In the present study, these data were analyzed by TVFM taking into account the chemical and phase composition of the samples derived from various precursors. We plotted methane adsorption values measured for the studied AC series at the temperature of 303 K and pressures 0.1, 3.5, and 10 MPa as a function of the basic TVFM parameters: characteristic energy of adsorption E_0 (Fig. 8(a)) and micropore volume W_0 (Fig. 8(b)).

As can be seen from Figs. 8(a) and (b), data points can be fitted by linear approximation in coordinates of the D-R equation (Eq. (4)), which is consistent with the mechanism of volume filling of micropores. The observed variations in the slope of these lines with an increase in pressure reflect changes in the relative contribution of the SEC to the adsorption capacity of the AC samples. The decrease in the slope of the $lg(a)=f(E_0^{-2})$ plot to zero with increasing pressure (see Fig. 8(a)) results from the reduced influence of adsorbate-adsorbent interactions on methane adsorption. The high-pressure methane adsorption capacity of microporous adsorbents is a strong function of micropore volume. A linear trend in the relationship between micropore volume and gravimetric methane adsorption capacity in carbon adsorbents prepared by different methods from various precursors was also shown in [5]. Therefore, if a pore size exceeds the doubled diameter of a methane molecule, the density of adsorbed methane is reduced. In addition, the influence of the pore size distribution on the methane adsorption should be taken into account [17,79].

To obtain a clearer picture of the impacts of the physicochemical properties of the studied adsorbents on the methane adsorption capacity, we plotted histograms of the absolute methane adsorption at 303 K and 0.1, 3.5, and 10 MPa (see Fig. 9(a), (b)). These histograms were analyzed in terms of TVFM, taking into account chemical and phase composition of the prepared ACs. The pressures were selected based on the following considerations. The value of 0.1 MPa corresponds to an average level of minimal residual pressure, P_X, in an ANG system and determines the deliverable capacity [1-5]. The deliverable capacity of the ANG system can be maximized by selecting an adsorbent with the lowest possible methane storage capacity at P_X. The values of 3.5 and 10 MPa are the maximal operational pressures (P_W), which ensure the highest efficiency of the ANG system [3].

As follows from Fig. 9(a), in the range of pressure close to atmospheric value, the maximum methane adsorption capacity is observed for the adsorbents with a high characteristic energy of adsorption (see Table 1): P-10 ($2x_0$=0.8 nm), T-6 ($2x_0$=1.3 nm), and C-7 ($2x_0$=1.0 nm). At high pressure (Fig. 9(b)), when the micropore volume plays a crucial role in the methane uptake, highly microporous samples display the best properties. Indeed, the furfural-based P-300 ($2x_0$=1.8 nm) and coconut-derived C-1 ($2x_0$=1.2 nm) adsorbents with the high micropore volume exhibit the maximum methane uptake despite very low characteristic energy of adsorption E_0. Among the peat-based carbons, T-6 ($2x_0$=1.3 nm) with a significant micropore volume, shows the highest methane adsorption capacity. Thus, it seems that the histograms can be interpreted

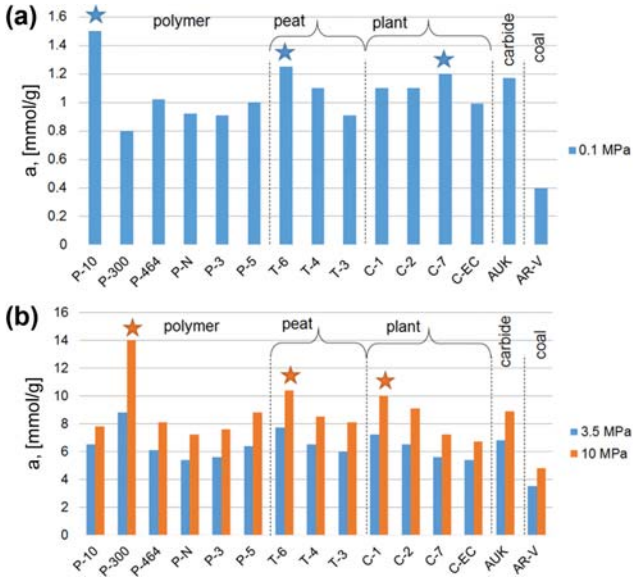

Fig. 9. Absolute methane adsorption in carbon adsorbents at the temperature of 303 K and pressures of (MPa): 0.1 (a), 3.5, and 10 (b). Stars indicate the AC samples with the highest methane adsorption capacity for each series.

in terms of SEC within the framework of only TVFM, disregarding the nature of the precursor. This is also evidenced by Figs. 8(a) and (b). However, several essential facts deserve particular attention. Although P-10 ($2x_0$=0.8 nm) and AUK ($2x_0$=0.8 nm) are characterized by close values of E_0 and W_0 (see Table 1), these adsorbents differ significantly from each other in methane adsorption capacity both at low and high pressures. A similar situation is observed for the pair of T-4 ($2x_0$=1.16 nm) and P-N ($2x_0$=1.16 nm), prepared from different raw materials.

Another example is C-EC ($2x_0$=1.0 nm), which possesses the highest value of E_0 for the C-series (see Table 1). At the same time, C-EC has the lowest adsorption capacity in the entire pressure range. One can explain these facts taking into account that at low pressures, the adsorption behavior of adsorbents with relatively small micropore volume is determined mainly by surface chemistry, which affects the binding energy between methane molecules and pore walls. According to the SEM-EDX data, the content of heteroatoms in P-10 exceeds significantly that in AUK (see Table 2). Despite the high uncertainty of the EDX analysis, we suggest that the presence of different heteroatoms, which form surface functional groups, affects the density of adsorption sites for methane. Therefore, the heterogeneous elemental composition is a significant factor explaining better adsorption property of P-10 compared to AUK at low pressure. Similarly, various impurities, including K, S, Si, Al, Cl, Ca, and Fe, which serve as potential high-energy adsorption sites in T-4, may be responsible for its higher methane adsorption capacity compared to P-N.

The histograms of methane adsorption at low and high pressures (Figs. 9(a) and (b)) enabled us to compare the efficiency of the activated carbons differing in precursor and activation methods as an adsorbent in the ANG systems. The deliverable adsorption capacity of the ANG system was calculated as a difference

Table 4. Methane storage and deliverable capacity of activated carbons

Precursor	Sample (activation)	Storage/Deliverable capacity, [mmol/g]		Temperature, [K]	Reference
		3.5 MPa	10 MPa		
Polymer	P-10	6.5/5.0	7.8/6.3	303	This work
	P-N	5.4/4.5	7.2/6.3	303	This work
	P-300	8.8/8.2	14.0/13.2	303	This work
	P-3	5.6/4.7	7.6/6.7	303	This work
	P-464	6.1/5.0	8.1/7.1	303	This work
	P-5	6.4/5.0	8.8/7.8	303	This work
	KUPO16-2-750 (KOH)	10.9/-	13.2/-	298	[44]
Peat	T-3	6.0/5.0	8.1/7.2	303	This work
	T-6	7.7/6.5	10.4/9.1	303	This work
	T-4	6.5/5.4	8.5/7.4	303	This work
	RB3 (steam)	4.7(at 3.0 MPa)/-	-/-	298	[31]
Vegetable	C-1	7.2/6.1	10.0/8.9	303	This work
	C-2	6.5/5.4	9.1/8.0	303	This work
	C-7	5.6/4.4	7.2/6.0	303	This work
	C-EC	5.4/4.41	6.7/5.71	303	This work
	CAQF-30 (TCA+VGA)	6.8/6.2	7.6/6.9	303	[40]
Carbide	AUK	6.8/5.63	8.9/7.73	303	This work
	DUT-38-A-950-4 (CO_2 VGA)	10.6/-	16.0 (8.5 MPa)/-	303	[51]
Mineral coal	AR-V	3.5/3.1	4.8/4.4	303	This work
	Discard coal-derived AC (KOH TCA)	15.0/13.1	-/-	303	[47]

between the adsorption values at an operational pressure of 3.5 or 10 MPa and the residual pressure of 0.1 MPa [2]. Table 4 summarizes the storage and deliverable capacities of the AC-series. The data of each AC series are compared with that reported by other authors for carbon adsorbents prepared from the same type of precursor. The type of activation of is indicated in brackets.

As seen from Table 4, the sorption properties of most ACs are comparable with those of carbon adsorbents reported in the literature. The P-300 sample prepared from furfural through the WGA process with the lowest methane adsorption capacity at P_X=0.1 MPa and relatively high methane uptake at P_W>3 MPa is the most efficient adsorbent among those considered in this study (see Figs. 9(a) and (b), Table 4). Thus, its deliverable methane adsorption capacity at 3.5 and 10 MPa is ~8.2 mmol/g and 13.2 mmol/g. The methane storage capacity of P-300 even slightly exceeds the value reported for the carbon adsorbent prepared by a multi-stage TCA technique from hypercrosslinked polymers, KUPO16-2-750 [44]. The KUPO16-2-750 has almost the same micropore volume as P-300: 0.93 cm^3/g, and exceeds P-300 in the BET surface and total pore volume: 2,500 m^2/g and 1.03 cm^3/g. It differs from P-300 by microporosity (W_{me}=0.11 cm^3/g). Under the same conditions, the chemically heterogeneous T-6 sample, which is the most effective adsorbent at low pressures, has the smallest storage and deliverable adsorption capacity. The C-1 carbon is the best in the C-series; it displays comparable methane adsorption performance with the CAQF-30 carbon prepared by chemical $ZnCl_2$ activation followed by steam activation [40]. The CAQF-30 has a higher BET surface and micropore volume than C-1: 2,114 m^2/g and 1.142 cm^3/g.

As seen from Table 4, carbide-derived AR-V displays the lowest storage and deliverable methane adsorption capacity when compared to other activated carbons. The main reason for the poor performance of this carbon is the low volume of relatively wide micropores. Nevertheless, activated carbon with a large micropore volume of 1.25 cm^3/g can be obtained from mineral coal through chemical activation [47].

The monolithic carbide-derived AUK with a high packing density displays less gravimetric storage and deliverable capacity than the solid spherical monodispersed granules of P-300. Note that the packing density is a crucial factor for another essential parameter characterizing the efficiency of the ANG systems, namely, the volumetric adsorption capacity of the adsorbent, which is beyond this study.

CONCLUSIONS

A series of AC adsorbents differing in raw materials and methods of their synthesis were examined to develop an efficient storage system for methane in the adsorbed state. The main parameters of their porous structure were calculated from the adsorption of standard benzene vapor within the framework of TVFM and BET method. It was found that the synthesis route with furfural as a precursor and vapor-gas activation yielded a microporous carbon adsorbent, P-300, with a large value of micropore volume of 0.89 cm^3/g and BET surface of 2,015 m^2/g.

The XRD and SEM data revealed that phase and chemical compositions, and surface homogeneity of the activated carbons were

determined by the type of precursor and conditions of activation. The obtained samples can be represented as graphitic crystallites of variable sizes and degree of crystallographic perfection, embedded into the amorphous matrix. XRD patterns and SEM-EDX data for the carbon adsorbents prepared from peat and mineral carbon revealed the presence of a significant amount of impurities inherited from precursors. Based on the SAXS data, the characteristic micropore sizes (radii of gyration) were calculated using cylindrical and slit-like models. The linear dependence between the radius of gyration and the micropore half-width determined from the standard benzene vapor adsorption data using TVFM was found for some carbons from thermo-reactive polymers and coconut shells. For most studied carbons, the radius of gyration is positively correlated with the pore sizes. The exceptions are the peat-derived adsorbents, whose porous structure results from thermochemical activation of extremely heterogeneous precursor material.

The approach based on TVFM enhanced by additional data on morphology and chemical composition of the adsorbents adequately describes the process of methane adsorption in carbon adsorbents of various genesis in the pressure range up to 10 MPa. Thus, the comparative analysis of methane adsorption capacity of the series of AC adsorbents in terms of their SEC values, morphology, and chemical composition revealed the main factors influencing their performance in ANG systems:

1. The efficiency of the AC adsorbents with a relatively homogeneous chemical composition is determined by the volume and width of micropores within a range of 0.8-1.2 nm, which provides the maximal density of adsorbed methane. This correlation was confirmed by the data on the highest methane uptake at low pressures (0.1 MPa) obtained for the adsorbents prepared from silicon carbide, PVDC, and coconut shell (AUK, P-10, and C-7).

2. Significant amounts of heteroatoms in the chemical composition of microporous carbon adsorbent inherited from the raw materials and activation procedure give rise to numerous high-energy adsorption sites, contributing to methane uptake at low pressures. As a result, peat-based carbons (T-6) demonstrate high adsorption capacity, although the micropore width (~1.3 nm) corresponds to the lowest calculated density of adsorbed methane.

3. The highest value of methane adsorption capacity at 3.5 and 10 MPa and relatively low methane uptake at 0.1 MPa ensured the maximal deliverable adsorption capacity of the P-300 adsorbent prepared from furfural *via* the vapor-gas activation. The large total pore volume of this adsorbent with sufficiently homogeneous chemical composition is supposed to be a crucial factor for methane adsorption at high pressures.

Thus, the adsorption behavior of each AC varied with pressure, and these variations depend on the chemical composition and porous structure. Therefore, an increase in the adsorption performance of the ANG system within the range of pressures up to 10 MPa requires the corresponding textural properties of adsorbents which should be optimized for thermodynamic operational conditions of ANG storage. The results obtained from this study can be important for developing a predictive algorithm for adsorption behavior of carbon adsorbents when choosing both a type of precursor and conditions of their preparation.

CREDIT AUTHOR STATEMENT

Ilya E. Men'shchikov: Conceptualization, Investigation; Visualization, Writing- Original draft preparation; **Andrey A. Shiryaev:** Methodology, Investigation; Writing - Review & Editing; **Andrey V. Shkolin:** Resources, Methodology, Investigation, Project administration; **Vladimir V. Vysotskii:** Investigation, Visualization; **Elena V. Khozina:** Writing-Original draft preparation, Writing-Reviewing and Editing; **Anatoly A. Fomkin:** Supervision, Project administration; Writing-Reviewing and Editing; Funding acquisition.

ACKNOWLEDGEMENTS

The investigations were carried out with the use of equipment of the Center of Physical Methods of Investigations of the A.N. Frumkin Institute of Physical Chemistry and Electrochemistry of Russian Academy of Sciences.

FUNDING

The research was carried out within the State Assignment of the Russian Federation (Project No. 01201353185) and the plan of the RAS Scientific Council (Theme No. 20-03-460-01).

NOMENCLATURE

A	: differential molar work of adsorption [kJ/mol]
a	: value of adsorption [mmol/g]
a_0	: limiting value of adsorption at the temperature T [K] [mmol/g]
E	: characteristic energy of gas adsorption [kJ/mol]
E_0	: characteristic energy of adsorption of standard vapor (benzene) [kJ/mol]
H_{CC}	: distance between centers of carbon atoms of pore walls [nm]
H_S	: average width of model slit-like micropores [nm]
I	: scattering intensity of x-rays at small angles [a.u.]
K	: coefficient of proportionality [dimensionless]
M	: molecular mass [g/mol]
m_0	: mass of regenerated adsorbent [g]
N	: total amount of gas introduced into the adsorption-measuring system [mmol]
n	: parameter in the Dubinin-Raduschkevich equation [dimensionless]
n	: exponent [dimensionless]
P	: pressure [Pa]
P_{cr}	: critical pressure [Pa]
P_S	: pressure of saturated vapors [Pa]
P_W	: maximal operational pressures of ANG system [Pa]
P_X	: minimal residual pressure of methane in ANG system [Pa]
q	: scattering vector [nm^{-1}]
R	: universal gas constant [J/(mol·K)]
R_G	: radius of gyration of micropores [nm]
R_{GS}	: radius of gyration of cross-section of a model cylindrical pore [nm]
R_T	: radius of gyration of a model slit-like pore [nm]
r	: radius of a crystallite [nm]

S_{BET} : BET specific surface area [m^2/g]
S_{me} : specific surface area of mesopores [m^2/g]
T : temperature [K]
T_{cr} : critical temperature [K]
T_0 : boiling point [K]
V : total geometric volume of adsorption measuring system [cm^3]
V_{ads} : volume of adsorbent with micropores [cm^3]
V_{He} : volume of adsorbent determined via helium pycnometry [cm^3]
W_{me} : specific mesopore volume [cm^3/g]
W_0 : specific micropore volume [cm^3/g]
W_S : specific total pore volume [cm^3/g]
x_0 : half-width of micropore [nm]
β : coefficient of similarity for the gas under study [dimensionless]
γ : ratio of crystallite radius to half-width of micropore [dimensionless]
δ_{gas} : density of gaseous phase [mmol/cm^3]
θ : angle of reflection (scattering) of X-rays in XRD (SAXS) [degrees]
λ : wavelength of x-rays [nm]
λ_{Cu} : wavelength of monochromatic CuKα-radiation [nm]
ρ_{CH4} : methane density in the slit-like pores with walls formed by graphene layers [g/cm^3]

Abbreviations

AC : activated carbons
ANG : adsorbed natural gas
EDX : energy dispersive x-ray analysis
PVDC : polyvinyl dichloride
PFR : phenol-formaldehyde resin
SAXS : small-angle x-ray scattering
SEC : structural and energy characteristics
SEM : scanning electron microscopy
TCA : thermochemical activation
TD : thermal decomposition
TVFM : theory of volume filling of micropores
VGA : vapor-gas activation
WVA : water vapor activation
XRD : x-ray diffraction

REFERENCES

1. A. Grint and S. T. Takagishi, Adsorbed Natural Gas (ANG) Research Conducted by Atlanta Gas Light Adsorbent Research Group (AGLARG). Final Report. (1990-1993). (Des Planes, IL: Gas Research Institute, End-Use Technology Development Division, 1994).
2. T. A. Makal, J.-R. Li, W. Lu and H.-C. Zhou, *Chem. Soc. Rev.*, **41**, 7761 (2012).
3. A. Y. Tsivadze, O. E. Aksyutin, A. G. Ishkov, I. E. Men'shchikov, A. A. Fomkin, A. V. Shkolin, E. V. Khozina and V. A. Grachev, *Russ. Chem. Rev.*, **87**, 950 (2018).
4. A. Y. Tsivadze, O. E. Aksyutin, A. G. Ishkov, M. K. Knyazeva, O. V. Solovtsova, I. E. Men'shchikov, A. A. Fomkin, A. V. Shkolin, E. V. Khozina and V. A. Grachev, *Russ. Chem. Rev.*, **88**, 925 (2019).
5. K. V. Kumar, K. Preuss, M. M. Titirici and F. Rodríguez-Reinoso, *Chem. Rev.*, **117**, 1796 (2017).
6. F. Rodríguez-Reinoso and K. Kaneko, in *Nanoporous materials for gas storage*, F. Rodríguez-Reinoso and K. Kaneko Eds., Springer Nature Singapore Pte Ltd, Singapore (2019).
7. A. A. Fomkin, A. A. Pribylov, A. G. Tkachev, N. R. Memetov, A. V. Melezhik, A. E. Kucherova, I. N. Shubin, A. L. Pulin, A. V. Shkolin, I. E. Men'shchikov, S. A. Zhedulov, K. A. Murdmaa and S. D. Artamonova, *Colloid J.*, **81**, 607 (2019).
8. A. Policicchio, E. Maccallini, R. G. Agostino, F. Ciuchi, A. Aloise and G. Giordano, *Fuel*, **104**, 813 (2013).
9. I. E. Men'shchikov, A. A. Fomkin, A. Y. Tsivadze, A. V. Shkolin, E. M. Strizhenov and E. V. Khozina, *Adsorption J.*, **23**, 327 (2017).
10. H. Tanaka, M. El-Merraoui, W. A. Steele and K. Kaneko, *Chem. Phys. Lett.*, **352**, 334 (2002).
11. M. D. Ganji, A. Mirnejad and A. Najafi, *Sci. Technol. Adv. Mat.*, **11**, 045001 (2010).
12. X. Zhu and Y. P. Zhao, *J. Phys. Chem. C*, **118**, 17737 (2014).
13. K. M. Anuchin, A. A. Fomkin, A. P. Korotych and A. M. Tolmachev, *Prot. Met. Phys. Chem. Surf.*, **50**, 173 (2014).
14. V. B. Fenelonov, Poristyi uglerod (Porous Carbon). Izd. Inst. Kataliza SO RAN, Novosibirsk (in Russian) (1995).
15. I. E. Men'shchikov, A. A. Fomkin, A. V. Shkolin, V. Yu. Yakovlev and E. V. Khozina, *Russ. Chem. Bull.*, **67**, 1814 (2018).
16. E. Mahmoud, *Surfaces*, **3**, 433 (2020).
17. S. Brunauer, P. H. Emmett and E. Teller, *J. Amer. Chem. Soc.*, **60**, 309 (1938).
18. M. Thommes, K. Kaneko, A. V. Neimark, J. P. Olivier, F. RodrõÂguez-Reinoso, J. Rouquerol and K. S. W. Sing, *Pure Appl. Chem.*, **87**, 1051 (2015).
19. M. M. Dubinin, *Prog. Surf. Memb. Sci.*, **9**, 1 (1975).
20. M. M. Dubinin, *Carbon*, **27**, 457 (1989).
21. A. G. G. Blanco, J. C. A. de Oliveira, R. López, J. C. Moreno-Piraján, L. Giraldo, G. Zgrablich and K. Sapag, *Colloids Surf. A Physicochem. Eng. Asp.*, **357**, 74 (2010).
22. R. Ruiz-Rosas, F. J. García-Mateos, M. C. Gutiérrez, J. Rodríguez-Mirasol and T. Cordero, *Front. Mater.*, **6**, 134 (2019).
23. V. Bernal, L. Giraldo and J. C. Moreno-Piraján, *J. Carbon Res.*, **4**, 62 (2018).
24. F. Rodriguez-Reinoso, in *Introduction to carbon technologies*, H. Marsh, E. A. Heintz and F. Rodriguez-Reinoso Eds., University of Alicante, Secretariado de Publicaciones, Alicante (1997).
25. F. Rodriguez-Reinoso, M. Molina-Sabio and M. T. Gonzalez, *Carbon*, **33**, 15 (1995).
26. M. Molina-Sabio, M. T. Gonzalez, F. Rodriguez-Reinoso and A. Sepúlveda-Escribano, *Carbon*, **34**, 505 (1996).
27. MOVE Program Overview. Advanced Research Project Agency, US DOE, 2012; https://arpa-e.energy.gov/sites/default/files/documents/files/MOVE Program Overview.pdf. Accessed 18.07.19.
28. T. S. Hui and M. A. A. Zaini, *Carbon Lett.*, **16**, 275 (2015).
29. M. T. Shirazani, H. Bakhshi, A. Rashidi and M. Taghizadeh, *J. Environ. Chem. Eng.*, **8**, 103910 (2020).
30. N. S. Nasri, H. U. Sidik, M. A. A. Zaini, N. M. Rashid, Z. A. Majid, S. Chelliapan, T. Kumar, H. M. Zain, R. Mohsin and N. Zaini, *Chem. Eng. Trans.*, **72**, 61 (2019).

31. A. Aleghafouri, M. Mohsen-Nia, A. Mohajeri, M. Mahdyarfar and M. Asghari, *Adsorpt. Sci. Technol.*, **30**, 307 (2012).
32. M. Bastos-Neto, D. V. Canabrava, A. E. B. Torres, E. Rodriguez-Castellón, A. Jiménez-López, D. C. S. Azevedo and C. L. Cavalcante Jr., *Appl. Surf. Sci.*, **253**, 5721 (2007).
33. E. M. Strizhenov, A. A. Fomkin, A. A. Zherdev and A. A. Pribylov, *Prot. Met. Phys. Chem. Surf.*, **48**, 614 (2012).
34. E. M. Strizhenov, A. V. Shkolin, A. A. Fomkin, A. A. Pribylov, A. A. Zherdev and I. A. Smirnov, *Prot. Met. Phys. Chem. Surf.*, **49**, 521 (2013).
35. A. A. Fomkin, A. A. Pribylov, K. O. Murdmaa, A. L. Pulin, A. V. Shkolin, I. E. Men'shchikov and S. A. Zhedulov, *Prot. Met. Phys. Chem. Surf.*, **55**, 413 (2019).
36. G. Sdanghi, S. Schaefer, G. Maranzana, A. Celzard and V. Fierro, *Int. J. Hydrogen Ener.*, In press (Available online 6 November 2019).
37. A. A. Fomkin, I. E. Men'shchikov, A. A. Pribylov, V. V. Gur'yanov, A. V. Shkolin, D. S. Zaitsev and A. V. Tvardovskii, *Colloid J.*, **79**, 144 (2017).
38. W. Djeridi, A. Ouederni, A. D. Wiersum, P. L. Llewellyn and L. El Mir, *Mater. Lett.*, **99**, 184 (2013).
39. K. C. Kemp, S. B. Baek, W. G. Lee, M. Meyyappan and K. S. Kim, *Nanotechnology*, **38**, 385602 (2015).
40. D. C. Azevedo, J. C. S. Araújo, M. Bastos-Neto, A. E. B. Torres, E. F. Jaguaribe and C. L. Cavalcante, *Micropor. Mesopor. Mater.*, **100**, 361 (2007).
41. J. E. Park, G. B. Lee, S. Y. Hwang, J. H. Kim, B. U. Hong, H. Kim and S. Kim, *Appl. Sci.*, **8**, 1596 (2018).
42. V. M. Mukhin, A. V. Tarasov and V. N. Klushin, Aktivnye ugli Rossii (Activated Carbons of Russia), Metallurgiya, Moscow (in Russian) (2000).
43. V. M. Mukhin, I. D. Zubova, V. V. Gur'yanov, A. A. Kurilkin and V. S. Gostev, *Sorbts. Khrom. Prots. (Sorp. & Chrom. Proc.)*, **9**, 191 (in Russian) (2009).
44. G. Gatti, M. Errahali, L. Tei, M. Cossi and L. Marchese, *Polymers*, **11**, 588 (2019).
45. N. Álvarez-Gutiérrez, M. V. Gil, M. Martinez, F. Rubiera and C. Pevida, *Energies*, **9**, 189 (2016).
46. D. Lozano-Castello, D. Cazorla-Amoros and A. Linares-Solano, *Energy Fuels*, **16**, 1321 (2002).
47. J. Abdulsalam, J. Mulopo, B. Oboirien, S. Bada and R. Falcon, *Int. J. Coal Sci. Technol.*, **6**, 459 (2019).
48. Y. Uraki, Y. Tamai, M. Ogawa, S. Gaman and S. Tokurad, *BioResources*, **4**, 205 (2009).
49. D. Bergna, T. Hu, H. Prokkola, H. Romar and U. Lassi, *Waste Biomass Valorization*, **11**, 2837 (2020).
50. S.-H. Yeon, S. Osswald and Y. Gogotsi, *J. Power Sources*, **191**, 560 (2009).
51. M. Oschatz, L. Borchardt, I. Senkovska, N. Klein, M. Leistner and S. Kaskel, *Carbon*, **56**, 139 (2013).
52. M. E. Casco, M. Martínez-Escandell and E. Gadea-Ramos, *Chem. Mater.*, **27**, 959 (2015).
53. A. P. Ramirez, S. Giraldo1, M. Ulloa, E. Flórez and N. Y. Acelas, *J. Phys.: Conf. Ser.*, **935**, 012012 (2017).
54. Z. Hu and M. P. Srinivasan, *Micropor. Mesopor. Mater.*, **43**, 267 (2001).
55. G. B. Kambarova and Sh. Sarymsakov, *Solid Fuel Chem.*, **42**, 183 (2008).
56. J. de D. López-González, F. Martínez-Vilchez and F. Rodríguez-Reinoso, *Carbon*, **18**, 413 (1980).
57. A. Aygün, S. Yenisoy-Karakaş and I. Duman, *Micropor. Mesopor. Mater.*, **66**, 189 (2003).
58. T. Zhang, W. P. Walawender and L. T. Fan, *Bioresour. Technol.*, **101**, 1983 (2010).
59. M. A. Tadda, A. Ahsan, A. Shitu, M. ElSergany, T. Arunkumar, B. Jose, M. A. Razzaque and N. N. N. Daud, *J. Adv. Civ. Eng. Pract. Res.*, **2**(1), 7 (2016).
60. P. J. Rangari and P. Chavan, *Int. J. Innov. Res. Sci. Eng. Technol.*, **6**(4), 5829 (2017).
61. J. J. Kipling and R. B. Wilson, *Trans. Farad. Soc.*, **56**, 557 (1960).
62. N. F. Fedorov, G. K. Ivakhnyuk, D. N. Gavrilov, V. V. Tetenov, G. N. Smetanin, V. V. Samonin, O. E. Babkin and Y. A. Zaitsev, in *Carbon adsorbents and their industrial applications*, Nauka, Moscow (1983).
63. N. F. Fedorov and V. V. Samonin, *Russ. J. Appl. Chem.*, **71**, 584 (1998).
64. A. V. Shkolin, A. A. Fomkin and V. A. Sinitsyn, *Colloid J.*, **70**, 849, (2008).
65. V. V. Sychev, A. A. Vasserman, V. A. Zagoruchenko, A. D. Kozlov, G. A. Spiridonov and V. A. Tzymarnyi, Termodinamicheskie svoistva metana (Thermodynamic properties of methane). Izdatelstvo Standartov, Moscow (in Russian) (1979).
66. L. A. Feigin and D. I. Svergun, *Structure analysis by small-angle x-ray and neutron scattering*, Plenum Press, New York and London (1989).
67. O. Glatter and O. Kratky, *Small-angle x-ray scattering*, Academic Press, London (1982).
68. A. A. Shiryaev, A. M Voloshchuk, V. V. Volkov, A. A. Averin and S. D. Artamonova, *J. Phys: Conf. Series*, **848**, 012009 (2017).
69. A. Guinier, *Ann. Phys.*, **11**, 161 (1939).
70. I. E. Men'shchikov, A. A. Fomkin, A. Y. Tsivadze, A. V. Shkolin, E. M. Strizhenov and A. L. Pulin, *Prot. Met. Phys. Chem. Surf.*, **51**, 493 (2015).
71. A. A. Fomkin, A. V. Shkolin, I. E. Men'shchikov, L. Pulin, A. A. Pribylov and I. A. Smirnov, *J. Meas. Techn.*, **58**, 1387 (2016).
72. A. A. Pribylov, V. V. Serpinskii and S. M. Kalashnikov, *Zeolites*, **11**, 846 (1991).
73. I. E. Men'shchikov, A. A. Fomkin, A. B. Arabei, A. V. Shkolin and E. M. Strizhenov, *Prot. Met. Phys. Chem. Surf.*, **52**, 575 (2016).
74. K. A. Rahman, W. S. Loh and K. S. Ng, *Procedia Eng.*, **56**, 118 (2013).
75. E. P. Barrett, L. G. Joyner and P. H. Halenda, *J. Am. Chem. Soc.*, **73**, 373 (1951).
76. A. M. Rutman and Y. A. Skakov, *Sov. Phys. Cryst.*, **34**, 338 (1989).
77. H. Fujimoto, *Carbon*, **41**, 1585 (2003).
78. M. M. Dubinin and G. M. Plavnik, *Carbon*, **6**, 183 (1968).
79. F. Rodríguez-Reinoso, C. Almansa and M. Molina-Sabio, *J. Phys. Chem. B.*, **109**, 20227 (2005).